Research Article Vol. 2, No. 7 / 15 Jul 2023 / Optics Continuum 1649
OPTICS CONTINUUM

Generation of Bessel-like beams with reduced sidelobes for enhanced light-sheet microscopy

JERIN GEOGY GEORGE,[1,*] KISHAN DHOLAKIA,[2,3,4] AND SHANTI BHATTACHARYA[1]

[1] Department of Electrical Engineering, IIT Madras, Chennai, India
[2] School of Physics and Astronomy, University of St. Andrews, St. Andrews KY16 9SS, UK
[3] School of Biological Sciences, University of Adelaide 5005, Australia
[4] Centre of Light for Life, University of Adelaide 5005, Australia
[*] ee20d029@smail.iitm.ac.in

Abstract: Bessel beams have found important applications due to their propagation invariant nature. However, the presence of sidelobes has proven a hindrance in key imaging and biophotonics applications. We describe the design and generation of sidelobe-suppressed Bessel-like beams (SSBB) that provide enhanced contrast for light-sheet imaging. The sidelobe suppression is achieved by the interference of two Bessel beams with slightly different wavevectors. Axicon phase functions for each Bessel beam are combined into a single phase function using the random multiplexing technique. This phase function is realised using a spatial light modulator to generate a SSBB. The generated beam at 633 nm has a $1/e^2$ radius of 44 μm and a propagation invariant distance of 39 mm which is more than four times that of the Rayleigh range of a Gaussian beam with the same $1/e^2$ radius. Within this distance, the overall peak intensity of the sidelobes of the SSBB is less than 10% that of the main lobe peak intensity. In addition, through numerical simulation for the recovery of spatial frequencies, we show that the SSBB improves image contrast compared to a Bessel beam for light-sheet imaging. We also show that the designed phase function can be realised using a meta-optical element.

1. Introduction

Bessel beams are of great interest due to their propagation invariant and self-healing properties [1–4]. While Bessel beams have opened up many possibilities in applications such as trapping and imaging [5–9], their high sidelobe energy limits their usability in such applications. A zeroth-order Bessel beam has a main central spot surrounded by concentric rings (sidelobes) of equal energy. Typically, the peak intensity of the first, second and third sidelobe of a zeroth-order Bessel beam is 16%, 9% and 6%, respectively [10,11]. In light-sheet fluorescence microscopy (LSFM), Bessel beams have been shown to possess superior properties when used in multi-photon modes due to the non-linear excitation [12–14]. However, linear excitation using one-photon Bessel beam in LSFM requires additional techniques such as confocal line detection or structured illumination to exploit its full potential [15–18]. These techniques can reduce the impact of sidelobes but require additional optical components, which can increase the size and complexity of the system. Hence, it is of interest to generate Bessel-like beams with reduced sidelobes in one-photon mode.

Surprisingly, limited research has been conducted to date to address this drawback. A study was performed in 2015 [10], where two Bessel beams were combined using an amplitude element comprising two annular slits. While this proved to be an effective way of achieving sidelobe suppression, the approach is inefficient, as the slits cut off most of the power of the incident beam. This technique was adopted and used by other researchers [19] for imaging in light-sheet microscopy. They used a spatial light modulator (SLM) in amplitude mode to generate a Bessel-like beam with reduced sidelobe amplitude, and thus energy. Another study [20] used a

#493003 https://doi.org/10.1364/OPTCON.493003
Journal © 2023 Received 13 Apr 2023; accepted 5 Jun 2023; published 30 Jun 2023

OPTICS CONTINUUM

genetic algorithm-generated phase profile for generating a sidelobe-suppressed 2D light-sheet. While this study is a phase-based approach and showed a reduction in the sidelobe near the central core, the design results in a 'perturbed phase profile' and is challenging to fabricate. Also, the generated beam has significant sidelobe intensity outside a small window.

In this paper, we propose a novel approach for designing a phase function that generates a sidelobe-suppressed Bessel-like beam (SSBB) while reducing overall sidelobe peak intensity. We present experimental results for the generation and analysis of the SSBB using a phase-only SLM. A major advantage of our approach is that the designed phase function can be converted into a diffractive/meta-optical element. Such an element can generate the SSBB with high efficiency and can be easily incorporated into optical systems. To demonstrate this capability, we provide preliminary experimental results for generating a SSBB using a meta-optical element. Furthermore, we discuss how the design parameters of our approach can be adjusted to achieve a better trade-off between the field of view (FOV) and image contrast in LSFM. We also quantify the spatial frequency extraction capability of the SSBB using the axial modulation transfer function (MTF) and show that the SSBB yields superior image contrast than a Bessel beam.

2. Sidelobe-suppressed Bessel-like beams

An ideal zeroth-order Bessel beam can be described by,

$$E(r,z) = A\,J_0(k_r r)e^{ik_z z}, \tag{1}$$

where J_0 is the Bessel function of zeroth-order, and k_r and k_z are the radial and longitudinal wavevectors. To reduce the sidelobe intensity, we use the technique mentioned in [10], the superposition of two Bessel beams with slightly different wavevectors (k-vectors). The interference of two Bessel beams has been studied previously [21,22], and it is shown that the resulting beam closely resembles each of the individual Bessel beams. The superposed beam can be represented by,

$$SP(r,z) = A_1\,J_0(k_{r_1} r)e^{ik_{z_1} z} + A_2\,J_0(k_{r_2} r)e^{ik_{z_2} z} \tag{2}$$

To reduce the sidelobes over a given propagation distance, the superposed beam's transverse intensity must be suppressed over the desired region and throughout the propagation distance. That means the Bessel beams' parameters (A_1, A_2, k_{r_1} and k_{r_2}) have to be optimised such that the following integral is minimised:

$$\int_{z_0}^{z_1}\int_{r_0}^{r_1} |SP(r,z)|^2 dr dz. \tag{3}$$

Here, r_0 to r_1 defines the transverse region, and z_0 to z_1 defines the propagation distance over which the sidelobes are suppressed. Minimising this integral means an overall reduction in the sidelobe energy, which in turn also reduces the peak intensity of the sidelobes. Another characteristic of the superposed Bessel beam is that its central core width oscillates, between the core widths of the individual Bessel beams, with a period given by [22]

$$p = \frac{2\pi}{|k_{z_1} - k_{z_2}|}. \tag{4}$$

The propagation invariant distance is defined as the region over which sidelobes remain below a desired limit, and it depends on the period ($\boldsymbol{p}$), which in turn depends on the radial wavevector ratio, $\boldsymbol{m = k_{r_1}/k_{r_2}}$. The propagation invariant distance increases with the period. However, as we can see from Eq. (4), the period increases for values of '$\boldsymbol{m}$' closer to 1, which results in a lower reduction in the sidelobes as the two Bessel beams become more similar. Previous studies [19] have reported that the reduction in sidelobes is better when '$\boldsymbol{m}$' is in the range of 0.4 to

OPTICS CONTINUUM

0.8, which we have also observed in our study. Thus, there is a trade-off between the sidelobe suppression and the propagation invariant distance.

In the next section, we discuss how the period and radial wavevector ratio affect the sidelobe peak intensity and the propagation invariant distance of the superposed beam.

2.1. Optimising the Bessel beam parameters

The optimised Bessel beam parameters (A_1, A_2, k_{r_1}, and k_{r_2}) can be obtained by minimising the integral in Eq. (3). The lower limit of the transverse suppression region (r_0) can be fixed as the desired core radius of the SSBB. The upper limit (r_1) is considered to be ten times the core radius, as the sidelobes outside this region are negligible. The lower limit for propagation region (z_0) is fixed to 0. The behaviour of the SSBB after a propagation distance '$\boldsymbol{p}$' will be the same because of the oscillatory nature that arises due to the periodically coinciding k_z vectors. The upper limit (z_1) is taken as 1/3 times the period '$\boldsymbol{p}$'. If we want a desired core radius for the SSBB, the individual Bessel beam parameters should also satisfy an additional constraint while optimising, given by the following relation [23],

$$r_0 = \frac{2.405}{wk_{r1} + (1-w)k_{r2}}, \tag{5}$$

where $w = \dfrac{A_1}{A_1 + A_2}$ and r_0 is the desired core radius of the SSBB. In this work, the core radius of the SSBB is set to 60 μm, which corresponds to a $1/e^2$ radius of about 44 μm. The depth of focus (DoF) of a Gaussian beam with the same $1/e^2$ radius is 19.22 mm. In this work, we design a phase function that generates an SSBB with a peak intensity of the sidelobes less than 10% the main lobe intensity while maximising the propagation invariant distance.

Initially, $\boldsymbol{m}$ is set to a fixed value while optimising Bessel beam parameters to observe its effect on sidelobe suppression and propagation invariant distance. Figure 1(a-d) shows the corresponding transverse intensity profile of the SSBB at the z = 0 plane. For $\boldsymbol{m}$ = 0.5, the first sidelobe peak intensity can be reduced to 2.52% at the z = 0 plane. In this case, other sidelobes appear in the outer regions and are more dominant than the first sidelobe. Even smaller values of $\boldsymbol{m}$ (less than 0.5) will further reduce the first sidelobe, but the propagation invariant distance will be reduced. When $\boldsymbol{m}$ is increased to 0.65, the first sidelobe peak intensity increases to 7.77% at the z = 0 plane. In this case, the first sidelobe is more dominant than other sidelobes. This happens because the two Bessel beams become more similar as $\boldsymbol{m}$ increases.

Figure 1(e) shows how the sidelobe peak changes with the propagation distance for different values of $\boldsymbol{m}$. Although the first sidelobe can be reduced to low values at the z = 0 plane with a relatively small $\boldsymbol{m}$ (less than 0.55), the propagation invariant distance is less. This is understandable because a lower value of $\boldsymbol{m}$ means comparatively different Bessel beams are being superposed, giving a better destructive interference of the sidelobes. However, the rapid relatively varying k_z vectors of the Bessel beams reduce this suppression effect to a small region. As $\boldsymbol{m}$ increases, the first sidelobe peak at z = 0 increases, but their rate of increase is low with propagation distance. When $\boldsymbol{m}$ exceeds 0.72, the first sidelobe becomes greater than 10% (our desired limit) at z = 0 itself. This is because the Bessel beams are no longer much dissimilar, and the achievable destructive interference of the sidelobes is minimal. Axial intensity variation is also an essential consideration when designing these beams. Figure 1(f) shows how the axial intensity changes with propagation distance for different $\boldsymbol{m}$ and $\boldsymbol{p}$ values. Axial intensity is maximum at the z = 0 plane and decreases as propagation distance increases. The rate at which the axial intensity decreases is lower when $\boldsymbol{m}$ is increased. To experimentally demonstrate the generation of SSBB, we used m = 0.61 while optimising the Bessel parameters. This value is chosen, based on simulation, to limit sidelobe peak intensity to below 10% while maximising the

OPTICS CONTINUUM

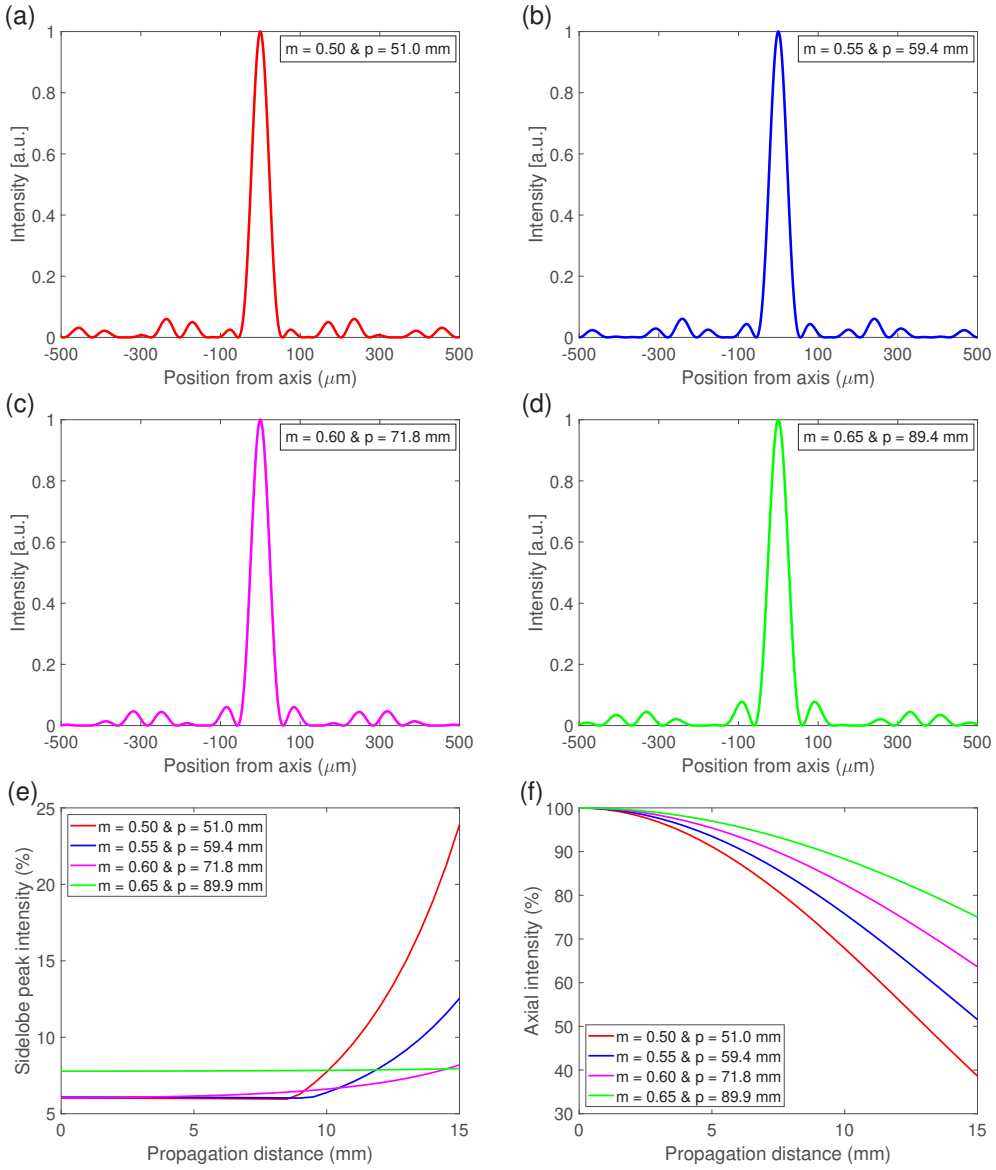

Fig. 1. Effect of the radial wavevector ratio (***m***) on sidelobe suppression of the SSBB. Corresponding value of period (***p***) is also given. (a-d) Transverse line intensity profile of the SSBB at z = 0 for different ***p*** and ***m***. (e) Sidelobe peak intensity of the SSBB in the transverse plane for different propagation distances. (f) The axial intensity of the SSBB for different propagation distances normalised against axial intensity at z = 0.

propagation invariant distance. The optimised Bessel beam parameters obtained for designing the phase function are $A_1 = 0.495$, $A_2 = 0.505$, $k_{r1} = 3.044 \times 10^4$ and $k_{r2} = 4.99 \times 10^4$.

2.2. *Designing a phase function to demonstrate sidelobe suppression*

Once the Bessel beam parameters for generating the SSBB are determined, the next step is to design the axicon phase function that generates the individual Bessel beams. The cone angle (θ)

OPTICS CONTINUUM

of a Bessel beam can be related to its wave vectors by the following relation,

$$\theta = \tan^{-1}\frac{k_r}{k_z}. \tag{6}$$

The cone angle of the Bessel beam is also related to the opening angle (α) of the axicon by,

$$\theta = (n-1)\alpha \tag{7}$$

By using these relations, the opening angle of the axicons α can be matched with the optimised k_r values. For the k_r values obtained, the opening angles of the axicon phase functions are 0.35^o and 0.58^o respectively. These phase functions are then spatially multiplexed by random multiplexing to synthesise the phase function for generating the SSBB. The multiplexing technique [24] combines the axicons after multiplying them with a random matrix consisting of 1s and 0s, which acts as a virtual mask. The transmittance of the mask is determined by the optimised Bessel parameters A_1 and A_2. These transmittance values may be further tuned to get the exact amplitudes at the superposition plane. This process is shown in Fig. 2.

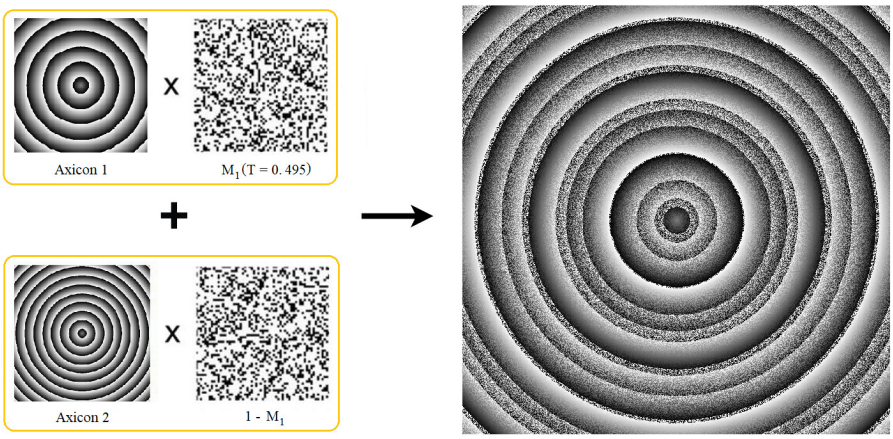

Fig. 2. Phase function for generating SSBB. The opening angle (α) for axicon 1 is 0.35^o and axicon 2 is 0.58^o. Transmittance of the virtual mask for axicon 1 is 0.495, and axicon 2 is 0.505.

The phase function (shown in Fig. 2) for generating SSBB is realised using an SLM. An SLM allows for the full wavefront control (0 to 2π) of the incident beam. However, due to the pixelation of the SLM, there will be unwanted zeroth-order light. To separate out the SSBB from the zeroth-order, a carrier frequency is added to the phase function to steer the desired beam away from the zeroth-order.

3. Results and discussion

3.1. Generation of SSBB using spatial light modulator

The experimental setup used to generate the SSBB is shown in Fig. 3. A collimated beam from a He-Ne laser source operating at a wavelength of 633 nm is expanded using a lens combination to illuminate the (phase-only) SLM exhibiting the designed phase pattern. A polariser is used after the lenses to select the horizontal polarisation required by the SLM. The SSBB generated at the near field is captured on a charge-coupled device sensor using a beam splitter and an iris.

As discussed in the previous section, the SSBB has a periodic nature along the direction of propagation, and the period of oscillation as per the design is $\approx$ 80 mm. This means the SSBB

OPTICS CONTINUUM

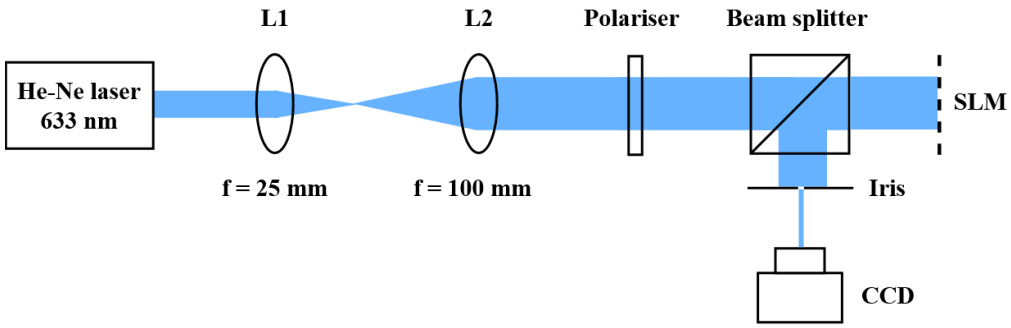

Fig. 3. Experimental setup for generating SSBB using SLM. Holoeye PLUTO SLM with a spatial resolution of 1920 X 1080 pixels is used for pattern generation. A BC106-VIS CCD camera with 6.45 µm X 6.45 µm pixel size is used to capture the SSBB.

will behave in a similar way at propagation distances that are multiples of the period as it does at the z = 0 plane. However, there is a limit to this behaviour determined by the depth of focus of the individual Bessel beams used for the superposition. The sidelobes of the SSBB are expected to be minimum at propagation distances which are multiples of this period. This is because the k_z vectors of the Bessel beams coincide at these planes allowing for better destructive interference. The sidelobes of the SSBB will also stay low at regions closer to these propagation distances. In our experiment, we chose propagation regions closer to 160 mm (twice the period) as this made the setting up of the optics easier. The experimental results of the SSBB and a Bessel beam with the same core radius are shown in Fig. 4.

The maximum sidelobe suppression and axial intensity for the experimentally generated SSBB are observed at a propagation distance of 163 mm from the SLM plane. The sidelobe peak intensity of the SSBB is only about 5.92% that of the main lobe peak intensity, unlike 13.36% in the case of the experimentally generated Bessel beam with a similar core radius. The $1/e^2$ radius of the SSBB at this propagation plane is measured to be 44 µm, which matches the designed value. The slight shift in the propagation distance at which the maximum sidelobe suppression and axial intensity are observed should be due to the variation in the experimentally achieved Bessel beam parameters compared to the optimised parameters. Moreover, the Bessel beam parameters (A_1 and A_2) will vary with propagation distance. But despite these issues, the generated SSBB is observed to have reduced sidelobes compared to a standard Bessel beam of the same core radius. To get a better comparison against the experimental results, the designed phase function is simulated using the Fourier beam propagation. In Fig. 5, the sidelobe peak intensity, the axial intensity and the effective beam radius of the experimentally generated beams are compared against the simulation results for different propagation distances around 163 mm.

The sidelobe peak intensity of the SSBB is within 10% that of the main lobe peak intensity for a propagation distance of 39 mm in the region between 143 mm to 182 mm (Fig. 5(a)). Figure 5(b) shows that the central core width of the SSBB is almost invariant (varying only 20%) in this propagation region. Beyond this distance, the sidelobe peak intensity increases further, and as the propagation distance becomes closer to the next period, it will again decrease. The effective beam radius variation of a Gaussian beam with the same $1/e^2$ radius is also plotted against the SSBB, and the SSBB exhibits superior propagation invariant nature. The depth of focus (DoF) of the Gaussian beam is only 19.22 mm. The axial intensity of the SSBB also decreases at a lower rate compared to an equivalent Gaussian beam (Fig. 5(c)). The experimental results are compared against the Fresnel diffraction simulation results. The deviations between the experiment and simulation results can be attributed to the zeroth-order not being entirely removed from the near-field in the experiment.

OPTICS CONTINUUM

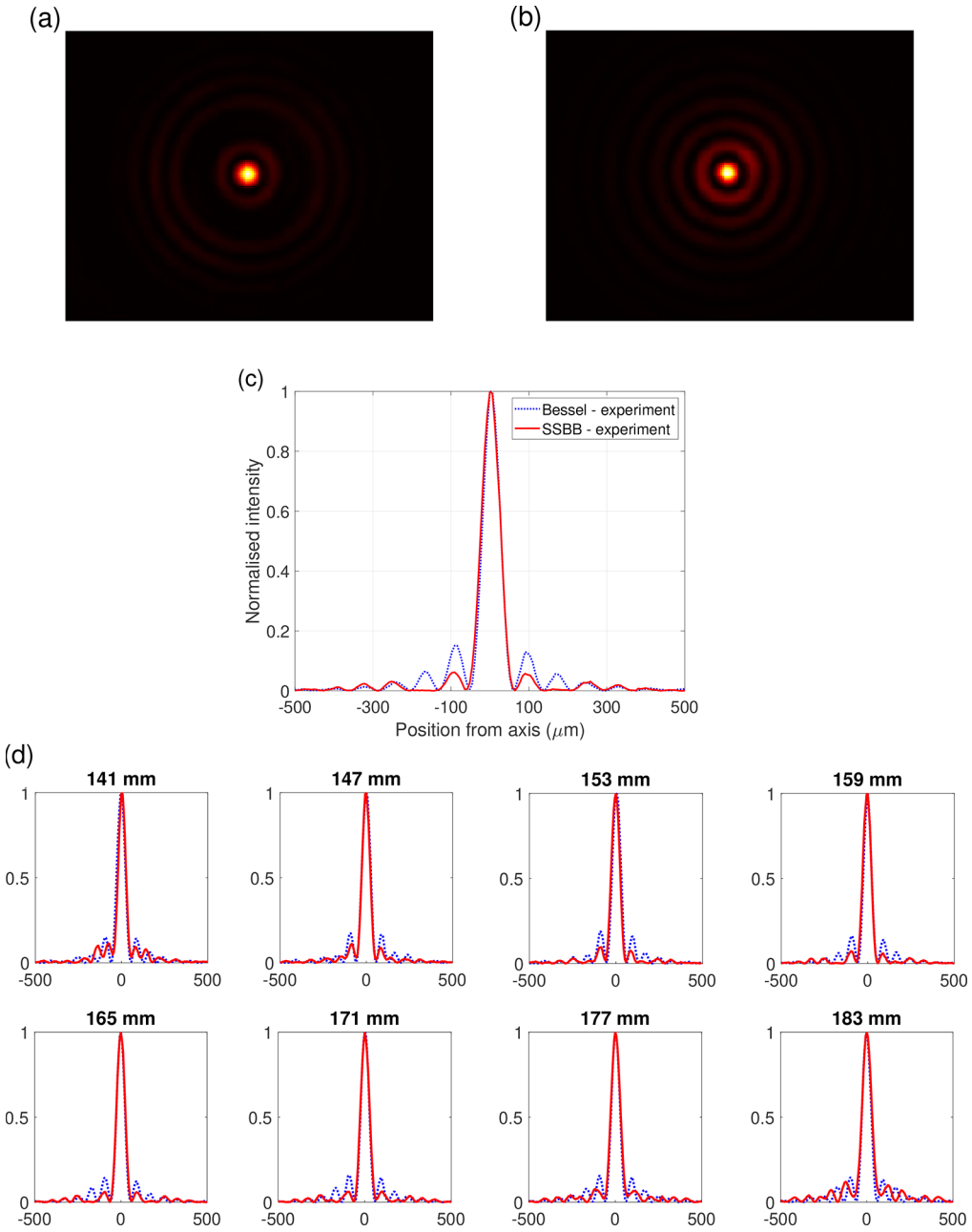

Fig. 4. Experimental results of the SSBB and Bessel beam generation using SLM - both beams are designed for a $1/e^2$ radius of 44 µm. (a-b) Cross-sectional intensity of the SSBB and Bessel beam respectively at z = 163 mm. (c) Intensity profile along the center of the SSBB and Bessel beam given in a and b. (d) Intensity profile along the center of the SSBB and Bessel beam at different propagation planes (141 mm to 183 mm).

OPTICS CONTINUUM

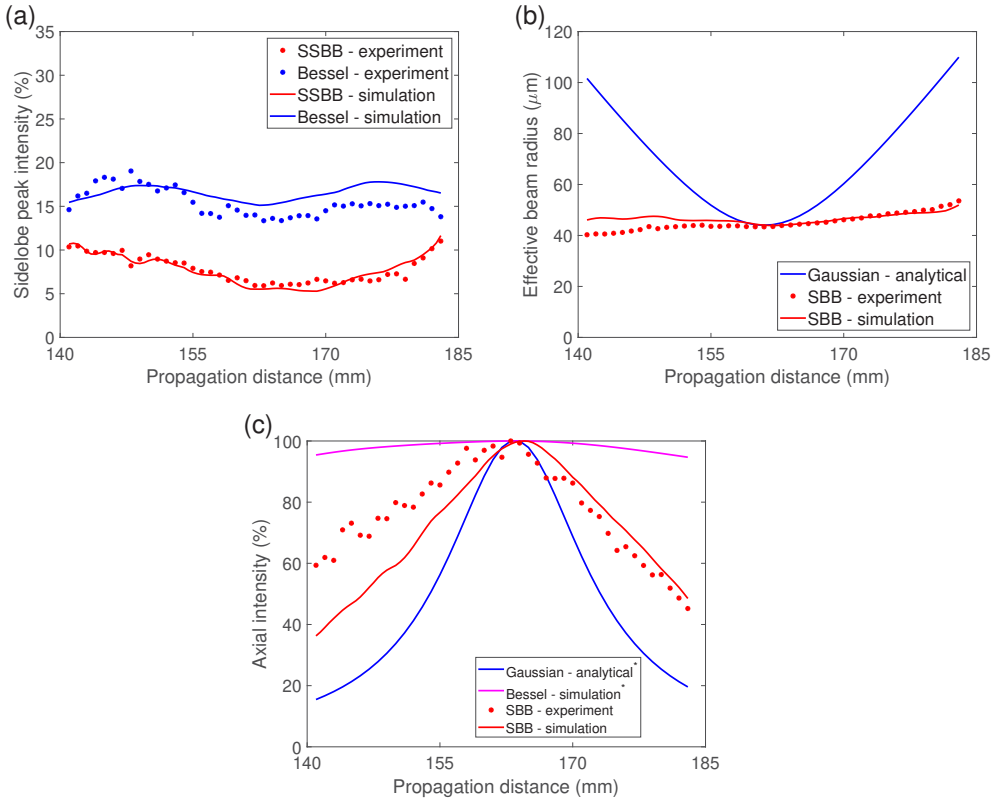

Fig. 5. Characterisation of the experimental and simulated SSBB and Bessel beam. (a) Sidelobe peak intensity of the SSBB and Bessel beam at different propagation planes of interest (centred around 163 mm). (b-c) $1/e^2$ radius and axial intensity of the SSBB and Bessel beam at different propagation planes compared against the analytical variation of an equivalent Gaussian beam. Axial intensity plot is normalised against the peak value in the propagation region. (* propagation distance corrected to show the fall of axial intensity)

3.2. Meta-optical element fabrication

To fabricate the meta-optical element, the designed phase function is digitised into 8 phase levels. Each of these phase levels is then realised using distinct poly-silicon cylindrical nanopillars which are spatially arranged according to the phase profile [25]. The design wavelength of the element is chosen as 1064 nm considering the complex refractive index of poly-silicon. Initially, a 500 nm-thick poly-silicon layer is deposited on quartz using low pressure chemical vapour deposition. Then a positive electron-beam resist (PMMA A8) is spin coated for the patterning process. The structure of the element is defined by electron-beam exposure followed by development using MIBK-IPA (1:3). A 40 nm aluminium layer is then deposited and the lift-off process is carried out using acetone. The aluminium layer left after the lift-off acts as a hard mask while transferring the pattern into the poly-silicon layer using inductively coupled plasma reactive ion etching. Finally, the aluminium mask is removed using wet etching. The process steps for the fabrication are shown in Fig. 6(a) and the scanning electron microscope images of the element fabricated are shown in Fig. 6(b). While optically characterising the element, we observed that energy is going to other diffraction orders. This is due to the fabrication imperfections in the element resulting in phase levels having values different from the designed ones. In order to filter out the other orders, we used a 4f system with a spatial filter in the Fourier plane after the first lens. After filtering, we

OPTICS CONTINUUM

were able to generate a SSBB with a sidelobe peak intensity of about 7.5% that of the main lobe peak intensity (Fig. 6(c)).

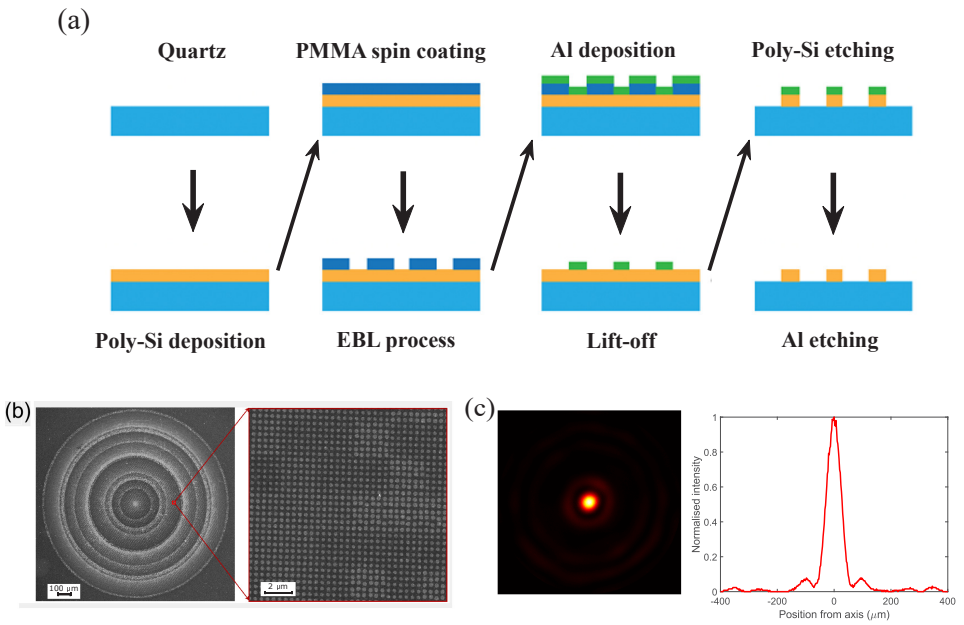

Fig. 6. Meta-optics for generating SSBB. (a) Fabrication process steps of the meta-optical element. (b) Scanning electron microscope images of the element (full element and zoomed-in view). (c) Cross-sectional and line intensity profile of the generated SSBB.

Although we generated a SSBB using meta-optics, the efficiency achieved was low due to fabrication imperfections. However, our phase function is similar to that of a meta-lens and there are several reports of such phase distributions being fabricated as meta-elements with high transmission efficiency (above 80%) [20,26–28]. With careful optimisation, the SSBB meta-element can also be realised with higher efficiency. This would be a huge improvement compared to the amplitude approach which suffers from high energy loss due to the blocking of most of the incident light.

4. Application to light-sheet imaging

We have conducted a simulation study to investigate the potential benefits of using (one-photon) sidelobe-suppressed Bessel beams for light-sheet imaging by comparing them with a Bessel beam of equivalent core radius. A wavelength of 488 nm and a core radius of 2.1 μm are selected for the study due to their practicality in light-sheet imaging. Light-sheet profiles for a SSBB and a Bessel beam are modelled using Fourier beam propagation (Fig. 7(a)). The resolution and contrast information of the two beams for light-sheet imaging is then determined from the modulation transfer function (MTF).

From the MTF plots (Fig. 7(b) and 7(c)), it can be seen that the SSBB is capable of resolving higher frequencies than a standard Bessel beam while maintaining the same contrast. Our simulations of light-sheets predict a maximum axial resolution of 5.4 μm and 11.11 μm for the SSBB and Bessel beams respectively, at 10% contrast.

OPTICS CONTINUUM

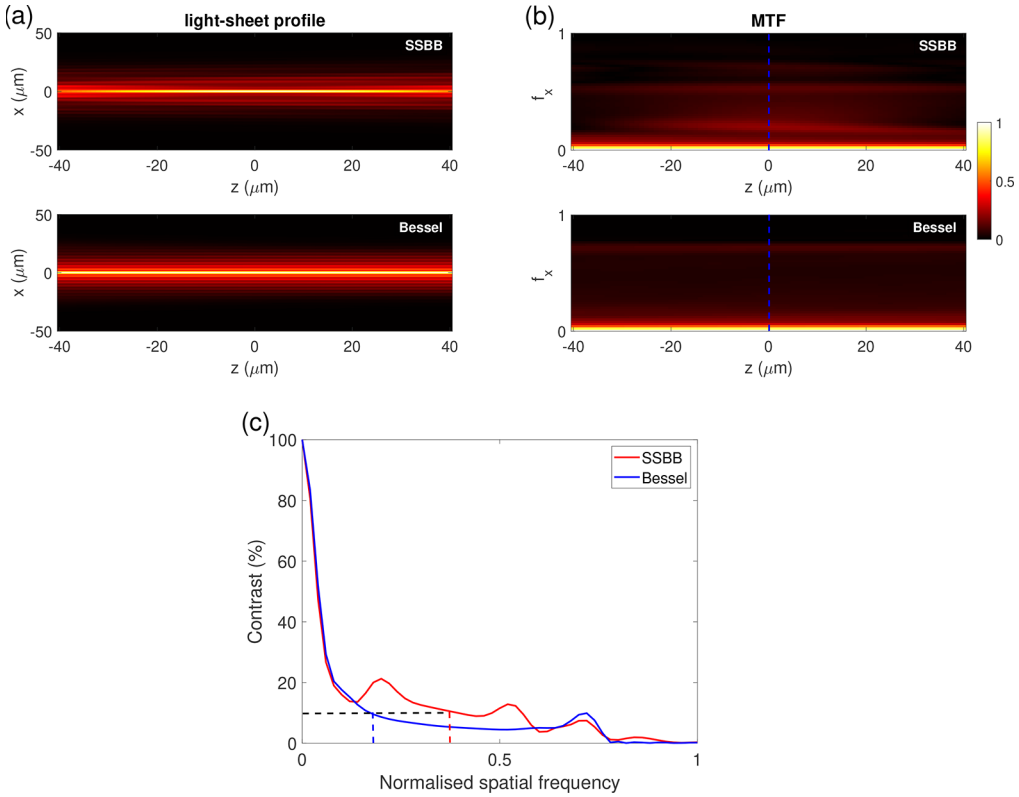

Fig. 7. Simulation of a SSBB and a conventional Bessel beam for light-sheet imaging. (a) x-z light-sheet cross sections of a SSBB and a Bessel beam using Fourier beam propagation. (b) Axial MTFs of the SSBB and Bessel beams. Spatial frequency (f_x) is normalised to $\frac{50}{L}$ (the contrast is less than 1% beyond this frequency); L = 100 μm. (c) MTF at z = 0 (blue dashed line in b).

5. Conclusion

We have designed and implemented a phase function on a spatial light modulator to generate a Bessel-like beam with reduced sidelobes. The SSBB exhibited a propagation invariant nature for a distance of more than twice the depth of focus of an equivalent Gaussian beam, which is four times the Rayleigh range. While the effective beam radius of an equivalent Gaussian beam increases by $\sqrt{2}$ times as it propagates to its Rayleigh range, the effective beam radius of the SSBB remains almost constant, varying only 20% within its propagation invariant region. The axial intensity decrease of the SSBB is also less compared to the Gaussian beam. We have shown that SSBB can be generated using meta-optics but our element requires further fabrication optimisation to achieve high efficiency. We have also performed a simulation study to explore the application of SSBB in light-sheet imaging. The results show an improvement in the image contrast for higher frequencies. However, this improvement comes at the expense of the FOV. Since the overall sidelobe energy in a SSBB is comparatively low, the photodamage in the sample will potentially be reduced [19]. A further attribute of our approach is that it is purely a phase approach, making it significantly more efficient than amplitude-based methods that employ similar suppression principles.

Funding. Scheme for Promotion of Academic and Research Collaboration (SPARC/2018-2019/P796/SL); Australian Research Council (FL210100099); H2020 Future and Emerging Technologies (EC-GA 863203).

OPTICS CONTINUUM

Acknowledgment. The authors acknowledge financial support from the Ministry of Human Resource Development, New Delhi through the SPARC project. KD acknowledges support from the Australian Research Council and the European Union's Horizon 2020 research and innovation programme under the H2020 FETOPEN project "Dynamic".

Disclosures. The authors declare no conflict of interest.

Data availability. Data underlying the results presented in this paper are not publicly available at this time but may be obtained from the authors upon reasonable request.

References

1. J. Durnin, J. Miceli Jr, and J. H. Eberly, "Diffraction-free beams," Phys. Rev. Lett. **58**(15), 1499–1501 (1987).
2. D. McGloin and K. Dholakia, "Bessel beams: diffraction in a new light," Contemp. Phys. **46**(1), 15–28 (2005).
3. L. Laycock and S. Webster, "Bessel beams-their generation and application," GEC Journal Research **10**, 36–51 (1992).
4. J. Arlt, V. Garcés-Chávez, W. Sibbett, and K. Dholakia, "Optical micromanipulation using a bessel light beam," Opt. Commun. **197**(4-6), 239–245 (2001).
5. T. Cizmar, V. Garces-Chavez, K. Dholakia, and P. Zemanek, "Optical trapping in counter-propagating bessel beams," in *Optical Trapping and Optical Micromanipulation*, vol. 5514 (SPIE, 2004), pp. 643–651.
6. S. N. Khonina, V. Kotlyar, R. Skidanov, V. Soifer, K. Jefimovs, J. Simonen, and J. Turunen, "Rotation of microparticles with bessel beams generated by diffractive elements," J. Mod. Opt. **51**(14), 2167–2184 (2004).
7. Y. Yang, Y.-X. Ren, M. Chen, Y. Arita, and C. Rosales-Guzmán, "Optical trapping with structured light: a review," Adv. Photonics **3**(03), 034001 (2021).
8. M. Mazilu, D. J. Stevenson, F. Gunn-Moore, and K. Dholakia, "Light beats the spread:non-diffracting beams," Laser Photonics Rev. **4**(4), 529–547 (2010).
9. L. Yi, L. Sun, and W. Ding, "Multifocal spectral-domain optical coherence tomography based on bessel beam for extended imaging depth," J. Biomed. Opt. **22**(10), 106016 (2017).
10. S. Mori, "Side lobe suppression of a bessel beam for high aspect ratio laser processing," Precis. Eng. **39**, 79–85 (2015).
11. F. He, J. Yu, Y. Tan, W. Chu, C. Zhou, Y. Cheng, and K. Sugioka, "Tailoring femtosecond 1.5-μm bessel beams for manufacturing high-aspect-ratio through-silicon vias," Sci. Rep. **7**(1), 40785 (2017).
12. A. Escobet-Montalbán, F. M. Gasparoli, J. Nylk, P. Liu, Z. Yang, and K. Dholakia, "Three-photon light-sheet fluorescence microscopy," Opt. Lett. **43**(21), 5484–5487 (2018).
13. B. Chen, X. Huang, D. Gou, J. Zeng, G. Chen, M. Pang, Y. Hu, Z. Zhao, Y. Zhang, and Z. Zhou, "Rapid volumetric imaging with bessel-beam three-photon microscopy," Biomed. Opt. Express **9**(4), 1992–2000 (2018).
14. F. M. Gasparoli, A. Escobet-Montalbán, J. Early, G. D. Bruce, and K. Dholakia, "Is laser repetition rate important for two-photon light sheet microscopy?" OSA Continuum **3**(10), 2935–2942 (2020).
15. F. O. Fahrbach and A. Rohrbach, "Propagation stability of self-reconstructing bessel beams enables contrast-enhanced imaging in thick media," Nat. Commun. **3**(1), 632 (2012).
16. T. A. Planchon, L. Gao, D. E. Milkie, M. W. Davidson, J. A. Galbraith, C. G. Galbraith, and E. Betzig, "Rapid three-dimensional isotropic imaging of living cells using bessel beam plane illumination," Nat. Methods **8**(5), 417–423 (2011).
17. L. Gao, L. Shao, C. D. Higgins, J. S. Poulton, M. Peifer, M. W. Davidson, X. Wu, B. Goldstein, and E. Betzig, "Noninvasive imaging beyond the diffraction limit of 3d dynamics in thickly fluorescent specimens," Cell **151**(6), 1370–1385 (2012).
18. R. M. Power and J. Huisken, "A guide to light-sheet fluorescence microscopy for multiscale imaging," Nat. Methods **14**(4), 360–373 (2017).
19. G. Di Domenico, G. Ruocco, C. Colosi, E. DelRe, and G. Antonacci, "Cancellation of bessel beam side lobes for high-contrast light sheet microscopy," Sci. Rep. **8**(1), 17178 (2018).
20. Y. Fan, M. K. Chen, and M. Qiu, *et al.*, "Experimental demonstration of genetic algorithm based metalens design for generating side-lobe-suppressed, large depth-of-focus light sheet," Laser Photonics Rev. **16**(2), 2100425 (2022).
21. S. Chávez-Cerda, M. Meneses-Nava, and J. M. Hickmann, "Interference of traveling nondiffracting beams," Opt. Lett. **23**(24), 1871–1873 (1998).
22. S. Chavez-Cerda, E. Tepichin, M. Meneses-Nava, G. Ramirez, and J. M. Hickmann, "Experimental observation of interfering bessel beams," Opt. Express **3**(13), 524–529 (1998).
23. J. G. George, Y. Guruvaiah, and S. Bhattacharya, "Sidelobe-suppressed bessel beam using hologram," in *Conference on Lasers and Electro-Optics/Pacific Rim*, (Optica Publishing Group, 2022), p. P_CTu8_24.
24. S. J. Lathika, V. Anand, and S. Bhattacharya, "A compact single channel interferometer to study vortex beam propagation through scattering layers," Sci. Rep. **10**(1), 296 (2020).
25. I. Staude, A. E. Miroshnichenko, M. Decker, N. T. Fofang, S. Liu, E. Gonzales, J. Dominguez, T. S. Luk, and D. N. Neshev, "Tailoring directional scattering through magnetic and electric resonances in subwavelength silicon nanodisks," ACS Nano **7**(9), 7824 (2013).
26. A. Arbabi, Y. Horie, M. Bagheri, and A. Faraon, "Dielectric metasurfaces for complete control of phase and polarization with subwavelength spatial resolution and high transmission," Nat. Nanotechnol. **10**(11), 937–943 (2015).
27. R. C. Devlin, M. Khorasaninejad, W. T. Chen, J. Oh, and F. Capasso, "Broadband high-efficiency dielectric metasurfaces for the visible spectrum," Proc. Natl. Acad. Sci. **113**(38), 10473–10478 (2016).

OPTICS CONTINUUM

28. Z.-B. Fan, Z.-K. Shao, M.-Y. Xie, X.-N. Pang, W.-S. Ruan, F.-L. Zhao, Y.-J. Chen, S.-Y. Yu, and J.-W. Dong, "Silicon nitride metalenses for close-to-one numerical aperture and wide-angle visible imaging," Phys. Rev. Appl. **10**(1), 014005 (2018).